

Dynamic population gratings in highly doped erbium fibers

Sonia Melle,^{1,*} Oscar G. Calderón,¹ Zhong C. Zhuo,^{1,2} Miguel A. Antón,¹ and Fernando Carreño¹

¹Escuela Universitaria de Óptica, Universidad Complutense de Madrid, Arcos de Jalón 118, Madrid 28037, Spain

²College of Physics, Jilin University, 2519 Jiefang Street, Changchun 130012, China

*Corresponding author: smelle@fis.ucm.es

Received April 15, 2011; accepted May 3, 2011;
posted May 12, 2011 (Doc. ID 146017); published June 7, 2011

The efficiency of the dynamic population gratings recorded in highly doped erbium fibers has been studied. We find that the grating response increases with optical density, although the presence of erbium ion pairs in fibers with ion density of the order of $6.3 \times 10^{25} \text{ m}^{-3}$ degrades the grating efficiency. The experimental results have been reproduced including inhomogeneous upconversion processes in the nonlinear coupled-wave equations. © 2011 Optical Society of America

OCIS codes: 190.4370, 060.2410.

1. INTRODUCTION

Dynamic gratings can be recorded in an erbium-doped fiber (EDF) by two counterpropagating coherent laser beams resonant with the transition between the ground and the metastable states of the erbium ions. The grating is produced through a spatial saturation of the fiber absorption in the maxima of the interference pattern. Since this process is associated with a redistribution of the population between both states, these dynamic gratings can be addressed as dynamic population gratings. The two beams that counterpropagate along the fiber are self-diffracted in the recorded grating via a two-wave mixing (TWM) process. These diffracted waves add in phase to the incident waves so the intensity of both transmitted beams increases. The first experimental observation of dynamic gratings recorded in EDFs was reported two decades ago by Frisken [1] and Fischer *et al.* [2]. In these works an additional incoherent probe beam in a four-wave mixing configuration was used to read the dynamic grating. Later on, applications of such gratings in single-frequency cw fiber lasers [3], in tunable narrowband fiber filters [4], and in adaptive interferometry [5] have been proposed.

An intense amount of work has also been developed recently to characterize the efficiency of dynamic gratings recorded in EDFs (see review by Stepanov [6]) via TWM. Stepanov and Hernández [7] found that the grating formation rate decreases with ion concentration (for fibers with moderate concentration of erbium ions) due to spatial migration of excitation. Particular attention has been given to the significant phase contribution in the grating recorded with wavelengths belonging to the wings of the erbium fundamental absorption spectrum [8] or to the anisotropic grating recorded when two orthogonally polarized waves counterpropagate through a birefringent EDF [9]. This last phenomenon is related to polarization hole burning. García Casillas and Stepanov have experimentally demonstrated an effective population grating recorded in an ytterbium-doped fiber at 976 nm [10].

In this work, we study the effect of ion concentration in the dynamic population grating recorded in highly doped erbium fibers. In order to characterize the dynamic grating, we performed a transient TWM experiment. We analyze in detail the grating efficiency in terms of the increase in the transmitted signals due to the self-diffraction of the recording signals. We have also analyzed the grating formation time. The results are compared to the predictions of a coupled-mode model for the two counterpropagating beams. It is shown that inter-ion interaction effects play a significant role in the TWM process in the case of considering highly doped Er^{3+} fibers.

2. EXPERIMENTAL SETUP AND RESULTS

We consider the experimental setup depicted in Fig. 1(a). Two coherent laser beams (forward and backward beams) resonant with the transition between the ground $^4I_{15/2}$ and the metastable $^4I_{13/2}$ states of the erbium ions counterpropagate through an EDF. The beams are obtained from a pigtailed distributed feedback laser diode (Anritsu, GB5A016) operating at 1536 nm. The laser works with a current and temperature feedback (Thorlabs, ITC502), which allows the laser to be kept at room temperature. This laser beam is split into two beams: the forward and the backward beam. The forward beam is sent through a phase shifter (General Photonics, FPS-001-01), which is provided with a piezo driver (General Photonics, PCD-001-3). To control the piezo driver, we use a function generator (Agilent, 33220A) that induces a square phase modulation with a controllable phase jump. In our experiments we set the phase jump to π to produce a displacement of the recording interference patterns by half of its spatial period. Thus, the transmitted beams show transitory negative absorption peaks [5], which decay exponentially to the steady-state value with a characteristic recovery time (in the order of the lifetime of the metastable level $\tau_0 \simeq 10.5 \text{ ms}$ [6]). Therefore, we use a modulation period of 100 ms to ensure that the dynamic grating reaches its stationary amplitude between two consecutive jumps. Once the forward beam comes out the EDF, it is collected in port 3 of circulator

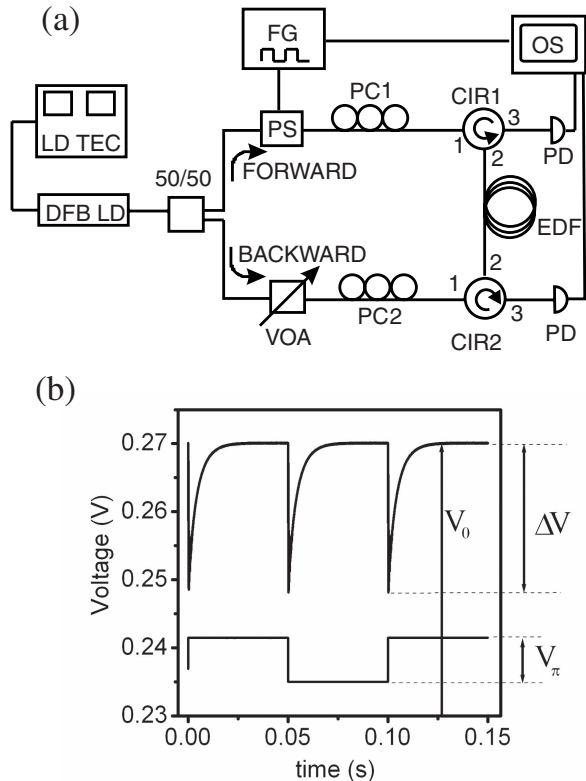


Fig. 1. (a) Experimental setup used to measure transient TWM in high-concentration EDFs. DFB LD, distributed feedback laser diode; LD TEC, laser diode and temperature controller; PS, phase shifter; FG, function generator; PC1 and PC2, polarization controllers; VOA, variable optical attenuator; CIR1 and CIR2, circulators; EDF, erbium-doped fiber; PD, photodetector; OS, oscilloscope. (b) Traces at the oscilloscope showing the backward transmitted signal in response to a square phase modulation with amplitude π introduced in the forward beam.

2 with a switchable-gain, amplified InGaAs photodetector (Thorlabs, PDA400) with 10 MHz bandwidth at the minimum gain setting. The backward beam counterpropagates through the EDF, and the output is sent to an identical photodetector at port 3 of circulator 1. An inline variable optical attenuator (Thorlabs, VOA50) is placed in the backward beam to equalize the forward and backward beam powers coming into the fiber. In addition, two polarization controllers (General Photonics, PLC-M02) at both inputs of the EDF are used to adjust the polarization of the two counterpropagating interacting beams and thus maximize the contrast of the interference pattern along the fiber. The change in the output power of both transmitted signals can be recorded simultaneously with a digital oscilloscope (Agilent, DSO9104A) and analyzed in a computer. We average the oscilloscope traces to avoid long-term temperature fluctuations in the output-recorded signals following the proposal of Stepanov *et al.* [5]. As an example, we show in Fig. 1(b) an average of 256 oscilloscope traces for the transmitted signal (top signal) in response to the square phase modulation (bottom signal) induced in the forward recording beam. Even so, a small amplitude asymmetry for two modulation consecutive semiperiods is obtained in some particular cases (not shown). This asymmetry can be attributed to spurious interferences from residual reflections in the fiber connections and can be corrected by shifting the recorded trace by half of the modulation period and then subtracting

half of the value of this shifted trace from the initial recorded signal (see [7]). Furthermore, we subtract from the symmetric backward (forward) transmitted signal the background signal obtained when only the forward (backward) beam propagates through the EDF.

With the aim of revealing the effect of ion concentration in the dynamic gratings, we consider several single-mode Al_2SiO_5 -glass-based EDFs (provided by Liekii, Ltd.). The properties of the fibers are listed in Table 1. These are not polarization-preserving fibers, and all of them have the same nominal mode field diameter at 1550 nm ($6.5\ \mu\text{m}$), the same fiber cladding ($245\ \mu\text{m}$), and the same numerical aperture (0.2). The level of doping ranges from 1.6 to $6.3 \times 10^{25}\ \text{m}^{-3}$ and the optical density varies from 3.8 to 17.5.

First, we analyze in detail the grating efficiency in terms of the relative amplitude of the transitory negative peaks induced in the transmitted beams ($\Delta V/V_0$). In Fig. 2(a), we plot the experimental dependence of the TWM relative amplitude on the recording input power for fibers with an ion density smaller than $2.7 \times 10^{25}\ \text{m}^{-3}$ (left) and for fibers with higher doping level (right). A maximum TWM relative amplitude is obtained when the input power is close to the power at which the fiber is saturated along its whole length. This effective saturation power increases with optical density as expected [see Fig. 2(b)]. Furthermore, the maximum relative amplitude response obtained increases with optical density, although highly doped fibers with ion density of $6.3 \times 10^{25}\ \text{m}^{-3}$ exhibit lower TWM relative amplitudes than moderately doped fibers for similar values of optical densities. These results have been summarized in Fig. 2(c).

The decrease of grating efficiency found for the highly doped fibers Er80 could be related to excitation loss mechanisms that typically take place at such high doping levels. To test if excitation quenching occurs in these fibers, we have performed additional measurements of the backward fluorescence when only one of the beams propagates through the fiber. The results are plotted in Fig. 3 for fibers Er20-1.0 and Er80-0.3. We observe that the fluorescence amplitude grows with input power and saturates at high powers. The maximum fluorescence amplitude reached for high input powers is expected to be proportional to the population of the metastable level as predicted by the two-level model (see [7]). Furthermore, as we are computing fluorescence of the whole fiber, the maximum fluorescence amplitude should be proportional to optical density. Following this approach, we should get a fluorescence amplitude 1.2 times larger in fiber Er80-0.3

Table 1. Fiber Properties^a

Label	α_{peak} (dB/m)	N_T ($\times 10^{25}\ \text{m}^{-3}$)	α_0 (m^{-1})	$\alpha_0 L$
Er20-1.0	20	1.6	3.8	3.8
Er30-1.0	30	2.1	5.0	5.0
Er30-3.5	30	2.1	5.0	17.5
Er40-1.0	40	2.7	6.4	6.4
Er80-1.0	80	6.3	15.0	15.0
Er80-0.2	80	6.3	15.0	3.0
Er80-0.3	80	6.3	15.0	4.5
Er80-0.5	80	6.3	15.0	7.5
Er80-0.7	80	6.3	15.0	10.5

^a α_{peak} , nominal peak absorption at 1530 nm; N_T , ion density provided by the manufacturer; α_0 , unsaturated absorption coefficient; $\alpha_0 L$, optical density.

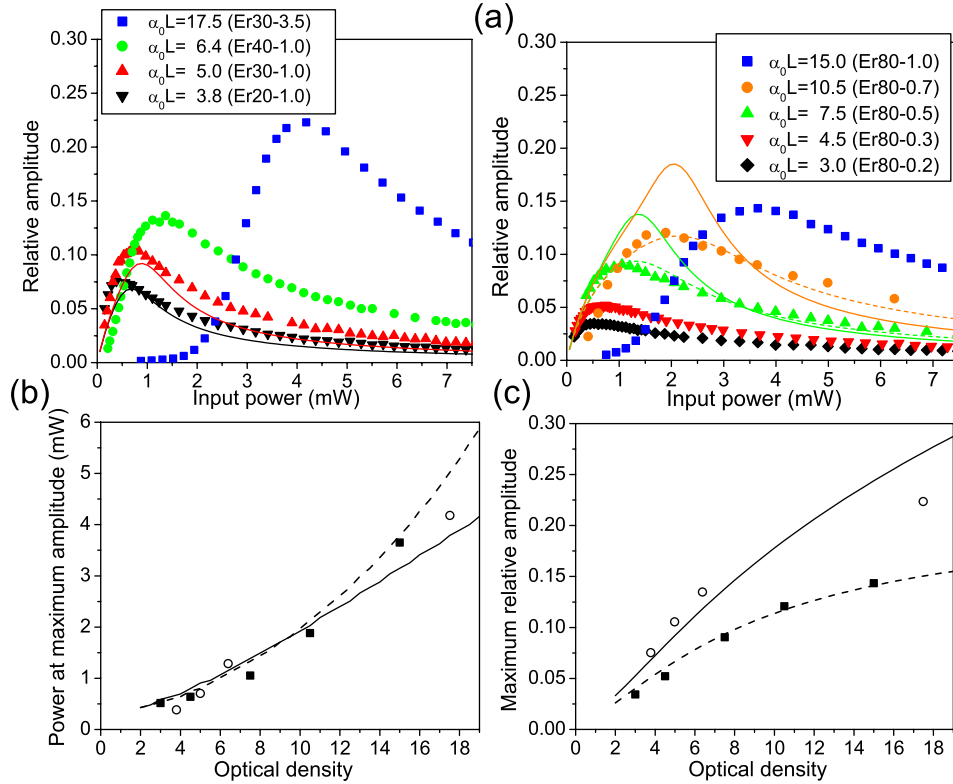


Fig. 2. (Color online) (a) Experimental relative amplitude as a function of input power for fibers with (left) moderate ion density ($\leq 2.7 \times 10^{25} \text{ m}^{-3}$) and (right) high ion density ($6.3 \times 10^{25} \text{ m}^{-3}$). (b) Power at the maximum relative amplitude and (c) maximum relative amplitude as a function of optical density for fibers with moderate ion density (circles) and with high ion density (squares). Solid curves, simulations with $\kappa = 0$; dashed curves, simulations with $\kappa = 0.25$.

than in fiber Er20-1.0, corresponding to the proportionality factor of both optical densities. However, we measure a quenching of the fluorescence of 16% for the fiber with higher ion density.

In order to test if the recorded gratings have any phase contribution, we measure the stationary TWM response inducing a sawtooth phase modulation (with amplitude 2π) in one of the recording beams to produce a frequency shift between

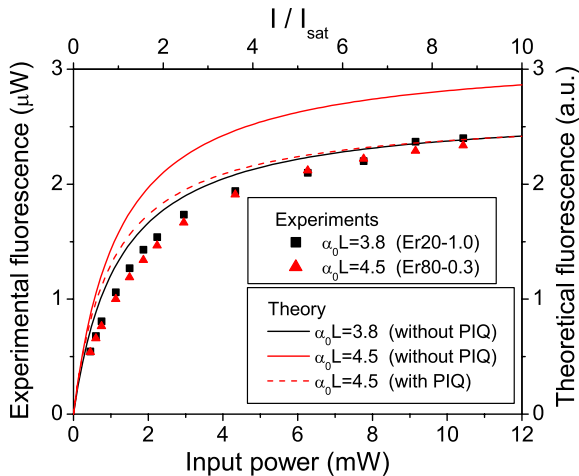


Fig. 3. (Color online) (Left/bottom axes) Experimental fiber fluorescence as a function of input power for two fibers with different optical density (symbols). (Right/top axes) Simulated fiber fluorescence given by Eq. (10) as a function of intensity I/I_{sat} (solid and dashed curves). In the case of the Er80-0.3 fiber, we plotted the results for $\kappa = 0$ (solid curves) and for $\kappa = 0.25$ (dashed curves).

both counterpropagating beams. As an example, the normalized stationary transmittance for the forward beam has been plotted in Fig. 4 as a function of the frequency offset for fibers Er20-1.0 [Fig. 4(a)] and Er80-0.3 [Fig. 4(b)]. We choose a forward beam input power close to the one at which the maximum relative amplitude response has been obtained (0.4 mW for Er20-1.0 and 0.6 mW for Er80-0.3). The expected symmetric Lorentz-like profile for an unshifted amplitude grating is obtained for the Er20-1.0, which agrees with the fact that the recording wavelength belongs to the central region of the absorption spectrum between the ground and the metastable state of the erbium ions [8]. Note that, for the highly doped fiber, a small transmission peak asymmetry is measured [see Fig. 4(b)], which could be attributed to a small phase contribution to the recording grating [11]. This small phase contribution will be further investigated elsewhere. Furthermore, when both counterpropagating beams are mutually coherent (zero frequency offset), an increase in transmission of 3% for fiber Er20-1.0 and 2% for fiber Er80-0.3 is obtained. Note that these values are roughly half of the transient TWM relative amplitude values obtained for these fibers [see Fig. 2(c)]. This is because, in the transient TWM experiment, the shifted interference pattern (by half of its wavelength) is in phase with the absorption grating recorded earlier so that light is absorbed more efficiently than when there is spatially uniform illumination with the same average level as occurs in the stationary transmittance [5].

Finally, we have analyzed the grating formation time (τ_g), that is, the decay time of the grating TWM transitory peaks, for fibers with different optical densities. The dependence of the

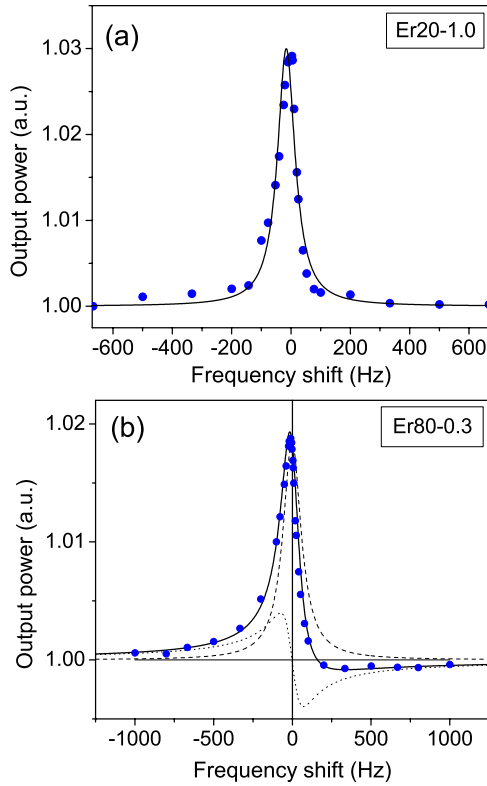


Fig. 4. (Color online) Normalized stationary transmittance for the forward beam as a function of the frequency offset for fiber (a) Er20-1.0 and (b) Er80-0.3: experimental data (symbols), theoretical fit (solid curve). (b) Lorentzian absorption curve showing partial amplitude-grating contribution (dashed curve) and Lorentzian dispersive curve showing phase-grating contribution (dotted curve).

inverse value of this time on the input power is plotted in Fig. 5. For fibers with moderate ion density ($\alpha_0 \leq 40$ dB/m), we observe that grating formation rate increases roughly linearly with input power as expected from the characteristic relaxation rate of the metastable state given by $\tau_0^{-1}(1+P)$, where P is the power normalized to the saturation power [see Fig. 5(a)]. Furthermore, a faster grating formation occurs as we decrease optical density since the effective power along the fiber increases. Similar behavior is found for fibers with high ion density [see Fig. 5(b)], although in this case the linear dependence of the grating formation rate with power shows higher slopes.

3. THEORETICAL MODEL AND RESULTS

In order to theoretically study the dynamic grating, we consider two coherent waves counterpropagating along the EDF: the forward and backward waves. These waves interact with the erbium ions and couple the ground state $^4I_{15/2}$ with the metastable state $^4I_{13/2}$. The total intensity I will be a sinusoidal interference pattern given by

$$\begin{aligned} I(z)/I_{\text{sat}} &= I_F + I_B + 2\sqrt{I_F I_B} m \cos(Kz) \\ &= I_0 \left(1 + \frac{2\sqrt{I_F I_B} m}{I_0} \cos(Kz) \right). \end{aligned} \quad (1)$$

Here I_F (I_B) is the intensity of the forward (backward) wave normalized to the saturation intensity $I_{\text{sat}} = \hbar\omega/(\tau_0(\sigma_a + \sigma_e))$, where ω is the frequency of both waves

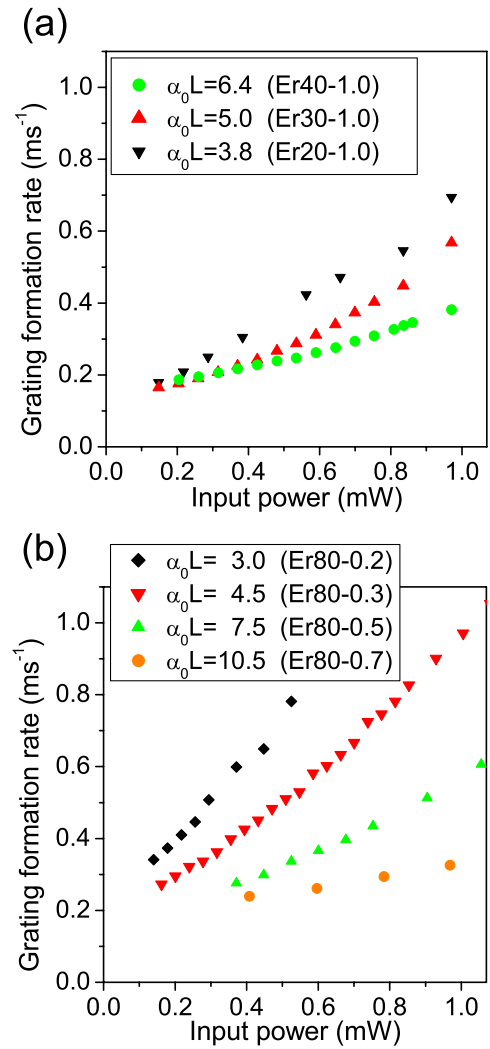


Fig. 5. (Color online) Experimental grating formation rate as a function of input power for fibers with (a) moderate ion density ($\leq 2.7 \times 10^{25} \text{ m}^{-3}$) and (b) high ion density ($6.3 \times 10^{25} \text{ m}^{-3}$).

(nearly resonant with transition $^4I_{15/2} \leftrightarrow ^4I_{13/2}$), τ_0 is the lifetime of the metastable state $^4I_{13/2}$, and σ_e and σ_a are the emission and absorption cross sections, respectively, at the light frequency ω . We assume equal cross sections, i.e., $\sigma_e \simeq \sigma_a$. $K = 2k$ is the spatial frequency of the pattern, k being the wavenumber of both waves, and m is a parameter that accounts for the contrast of the interference pattern. $I_0 = I_F + I_B$ is the average intensity along the fiber normalized to I_{sat} . This intensity pattern will induce a spatial profile in the optical absorption $\alpha = \alpha_0/(1 + I/I_{\text{sat}})$, where $\alpha_0 = \sigma_a N_T$ is the unsaturated absorption coefficient, being N_T the ion concentration. By assuming low contrast ($m \ll 1$), we can consider only the first spatial harmonic (Bragg grating component), i.e., $\alpha \simeq \bar{\alpha} - \delta\alpha \cos(Kz)$, where $\bar{\alpha}$ is the average fiber absorption and $\delta\alpha$ is the absorption grating amplitude, given by

$$\bar{\alpha} = \frac{\alpha_0}{1 + I_0}, \quad (2)$$

$$\delta\alpha = \frac{\alpha_0 2m\sqrt{I_F I_B}}{(1 + I_0)^2}. \quad (3)$$

We analyze the propagation of both counterpropagating waves by considering the nonlinear coupled-wave equations:

$$\frac{\partial E_F}{\partial z} = -\frac{\bar{\alpha}}{2}E_F + \frac{\delta\alpha}{4}E_B, \quad (4)$$

$$\frac{\partial E_B}{\partial z} = \frac{\bar{\alpha}}{2}E_B - \frac{\delta\alpha}{4}E_F, \quad (5)$$

where E_F (E_B) is the amplitude of the forward (backward) wave normalized to $\sqrt{2I_{\text{sat}}/(c\epsilon_0)}$; thus, $E_F^2 = I_F$ ($E_B^2 = I_B$). Finally, z is the spatial variable along the fiber (being the fiber length L). We numerically solve Eqs. (4) and (5) by using a standard Matlab function that implements a three-stage Lobatto IIIA [12]. Taking into account the boundary conditions $E_F(0) = E_B(L) = \sqrt{I_{\text{in}}}$, we calculate the output intensities $I_F(L) = I_B(0) = I_{\text{out}}$. Then, we compute the relative amplitude of the TWM as $(I_{\text{out}} - I_{\text{out}}^{\text{incoh}})/I_{\text{out}}$, where $I_{\text{out}}^{\text{incoh}} = I_F(L) = I_B(0)$ are the output intensities calculated when two incoherent waves counterpropagate along the fiber, that is, in the absence of the TWM. The predicted relative amplitude corresponds to the stationary TWM response, which is roughly half of the transient TWM relative amplitude value, as it was pointed out in Section 2.

In order to carry out the simulations, we first estimate the saturation intensity (I_{sat}) and the unsaturated absorption coefficient (α_0) for the different fibers. By fitting the experimental output–input power curve for the less-doped fiber (Er20-1.0) (not shown), we obtain a saturation power of $P_{\text{sat}} = 0.42$ mW, so that $I_{\text{sat}} = 1.27$ kW/cm² (where we used a mode field diameter of 6.5 μm). The insertion loss was estimated to be 0.8 and $\alpha_0 \simeq 3.8$ m⁻¹. With this value of α_0 , and taking into account the nominal ion densities provided by the manufacturer for the other EDFs (see Table 1), we estimate the unsaturated absorption coefficients listed in Table 1. The parameter m , which appears in Eq. (1) and that accounts for the contrast of the interference pattern, has been left free to fit the experimental TWM relative amplitude for the less-doped fiber (Er20-1.0). We obtain a value of $m = 0.055$. As an example, we plot in Fig. 2(a) (solid curves) the simulated relative amplitude as a function of the input power for some representative fibers. For moderate ion densities (left graph), the simulated curves agree with the experimental ones. However, we can observe that, for the fibers with higher ion density, the simulated curves overestimate the experimental TWM response (solid curves in right graph). These results can be clearly seen in Fig. 2(c), where the simulated maximum relative amplitude (computed from the previous curves) is plotted as a function of the optical density (solid curve). This curve reproduces well the experimental behavior for fibers with moderate ion concentration whereas deviates from the experimental behavior exhibited by highly doped fibers. In what follows, we will try to address this issue.

The degradation of the grating efficiency at very high doping levels could be attributed to inter-ion interaction effects that take place between neighboring ions in these fibers. Previous works have shown that upconversion processes via interparticle interactions are the main cause of gain degradation in EDF amplifiers [13,14]. In these processes one initially excited (${}^4I_{13/2}$) erbium ion (donor) donates its energy to a neighbor excited erbium ion (acceptor), producing one up-

converted ion and one ground-state ion (${}^4I_{15/2}$). The upconverted ion then relaxes rapidly to the initial excited state ${}^4I_{13/2}$. As a result of this interaction, one excited ion is lost. There are two different kinds of upconversion processes. The first one is the homogeneous upconversion in which the ions are uniformly distributed and the energy transfers from one ion to its neighbor with a characteristic time of a few milliseconds. The second one is the inhomogeneous upconversion or pair-induced quenching (PIQ) in which the ions are not uniformly distributed and the energy transfer happens between two adjacent excited paired ions with a characteristic time of a few microseconds. In the present case, we will consider that the PIQ is the dominant upconversion process in high-concentration EDFs [15].

Let us analyze the effect of PIQ on the TWM response. Following the model developed by Wysocki *et al.* [15] and Li *et al.* [16] to explain the effect of ion pairs on the output performance of EDF lasers, we group the erbium ions into two groups: isolated ions with an excited-state lifetime close to 10 ms and paired ions with a very fast decay of the pair excited state ${}^4I_{13/2}$ (close to microseconds). The isolated ions can be described by a two-level system, the ground state ${}^4I_{15/2}$ and the upper level ${}^4I_{13/2}$ with population densities N_1 and N_2 , respectively [see Fig. 6(a)]. Then, the rate equation for N_2 is

$$\frac{\partial N_2}{\partial t} = \frac{\sigma_a I}{\hbar\omega} (N_i - N_2) - \frac{\sigma_e I}{\hbar\omega} N_2 - \frac{1}{\tau_0} N_2, \quad (6)$$

where t is the time variable, $N_i = N_1 + N_2$ is the concentration of isolated ions, and I is the beam intensity. The characteristic relaxation rate of the metastable state is given by $\tau_0^{-1}(1 + I/I_{\text{sat}})$.

The ion pairs can be described as a three-level system: the ground state (${}^4I_{15/2}$, ${}^4I_{15/2}$), the intermediate level with one excited ion (${}^4I_{15/2}$, ${}^4I_{13/2}$), (${}^4I_{13/2}$, ${}^4I_{15/2}$), and the upper level (${}^4I_{13/2}$, ${}^4I_{13/2}$) with population densities $N_{1,\text{pr}}$, $N_{2,\text{pr}}$, and $N_{3,\text{pr}}$, respectively [see Fig. 6(b)]. For the sake of simplicity, and due to the fast decay of the upper level $N_{3,\text{pr}}$, we consider only the two lower levels. Then, the rate equation for the intermediate level $N_{2,\text{pr}}$ is

$$\frac{\partial N_{2,\text{pr}}}{\partial t} = \frac{2\sigma_a I}{\hbar\omega} (N_{\text{pr}} - N_{2,\text{pr}}) - \frac{\sigma_e I}{\hbar\omega} N_{2,\text{pr}} - \frac{1}{\tau_0} N_{2,\text{pr}}, \quad (7)$$

where $N_{\text{pr}} \simeq N_{1,\text{pr}} + N_{2,\text{pr}}$ is the concentration of pairs. The temporal dynamics of the excited state $N_{2,\text{pr}}$ [see Eq. (7)] exhibits a different characteristic relaxation rate in comparison to that of the isolated ions, i.e., $\tau_0^{-1}[1 + (\sigma_e + 2\sigma_a)/(\sigma_a + \sigma_e)I/I_{\text{sat}}]$. In particular, the linear dependence of this relaxation rate with the intensity shows a larger slope, which in fact could be related with the larger slope measured for the grating formation rate at high doping levels (see Fig. 5). The steady-state populations can be easily obtained from Eqs. (6) and (7) by setting the $\partial/\partial t = 0$:

$$N_2 = \frac{N_T(1 - 2\kappa)}{2} \frac{I/I_{\text{sat}}}{1 + I/I_{\text{sat}}}, \quad (8)$$

$$N_{2,\text{pr}} = N_T \kappa \frac{I/I_{\text{sat}}}{1 + (3/2)I/I_{\text{sat}}}. \quad (9)$$

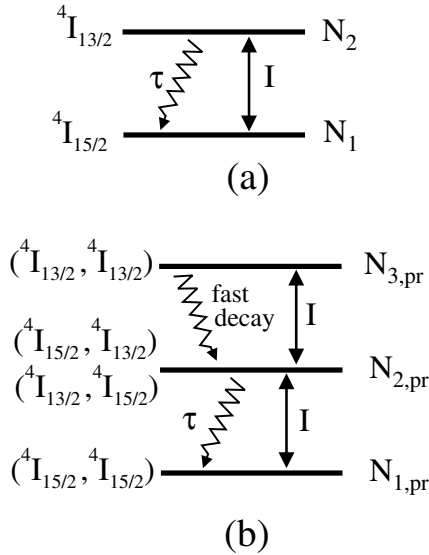


Fig. 6. (a) Two-level system for isolated Er ions with concentration N_i and (b) three-level system for Er ion pairs with concentration N_{pr} . The total concentration of ions is $N_T = N_i + 2N_{pr}$.

Here $\kappa = N_{pr}/N_T$ is the fraction of ion pairs in the total ion concentration ($N_T = N_i + 2N_{pr}$). The total excited population $N_2 + N_{2,pr}$ increases with beam intensity I and saturates to a maximum value of $(N_T/2)(1 - (2/3)\kappa)$ at high intensities (i.e., $I \gg I_{sat}$). This result clearly shows the excitation quenching due to inhomogeneous upconversion, i.e., the PIQ will reduce the efficiency of the fluorescence.

In order to compare with the experimental data shown in Fig. 3, we have roughly estimated the fluorescence signal emitted by the whole fiber as $I_f \propto L(N_2 + N_{2,pr})$:

$$I_f \propto \frac{LN_T}{2} \left[\frac{(1-2\kappa)I/I_{sat}}{1+I/I_{sat}} + \frac{2\kappa I/I_{sat}}{1+(3/2)I/I_{sat}} \right]. \quad (10)$$

Analytical results obtained from Eq. (10) have been plotted in Fig. 3 together with the experimental data measured for two fibers with different ion density. The value of κ is left to be a free parameter to reproduce the experimental fluorescence quenching observed for the highly doped fiber (Er80-0.3) (dashed curve), which results in $\kappa = 0.25$. This value is in accordance with the one used in previous works for similar doping levels [17]. We also plotted the case without PIQ, i.e., with $\kappa = 0$ (solid curves), for comparison purposes.

Let us now calculate how the optical absorption (α) reached in the stationary regime is modified when including PIQ effects:

$$\begin{aligned} \alpha &= \sigma_a N_1 - \sigma_e N_2 + 2\sigma_a N_{1,pr} \\ &= \frac{\alpha_0(1-2\kappa)}{1+I/I_{sat}} + \frac{\alpha_0 2\kappa [1 + (1/2)I/I_{sat}]}{1 + (3/2)I/I_{sat}}. \end{aligned} \quad (11)$$

This optical absorption presents the contribution of both isolated and paired ions. Note that the optical absorption due to the ion pairs [second term in Eq. (11)] does not saturate with beam intensity. This leads to a lower transmittance, especially at high intensities. As we mentioned above, the intensity pattern given by Eq. (1) will induce a spatial profile in the optical absorption: $\alpha \simeq \bar{\alpha} - \delta\alpha \cos(Kz)$, where the average fiber

absorption $\bar{\alpha}$ and the absorption grating amplitude $\delta\alpha$ now read

$$\bar{\alpha} = \frac{\alpha_0(1-2\kappa)}{1+I_0} + \frac{\alpha_0 2\kappa(1 + \frac{1}{2}I_0)}{1 + \frac{3}{2}I_0}, \quad (12)$$

$$\delta\alpha = \delta\alpha_i + \delta\alpha_{pr} = \frac{\alpha_0(1-2\kappa)2m\sqrt{I_F I_B}}{(1+I_0)^2} + \frac{\alpha_0 2\kappa 2m\sqrt{I_F I_B}}{(1 + \frac{3}{2}I_0)^2}. \quad (13)$$

This absorption grating presents the contribution of both isolated ions, with amplitude $\delta\alpha_i$ [first term on right-hand side of Eq. (13)], and paired ions, with amplitude $\delta\alpha_{pr}$ [second term on right-hand side of Eq. (13)]. If we analyze in detail this expression, we clearly see that the presence of clustered ions decreases the grating efficiency with respect to the case where all ions are isolated. Note that the grating amplitude of the paired ions normalized to the corresponding concentration of ions [$\delta\alpha_{pr}/(2N_{pr})$] is smaller than the one corresponding to the isolated ions ($\delta\alpha_i/N_i$) due to the nonsaturable absorption term. Therefore, the total energy of the diffracted beam decreases with respect to the case where only isolated ions are present.

Finally, in order to analyze the effect of PIQ in the TWM response, we study the propagation of both counterpropagating waves by considering the nonlinear coupled-wave Eqs. (4) and (5) and using a pair concentration of $\kappa = 0.25$. In Fig. 2(a) (right graph) we plot the simulated relative amplitude as a function of the input power for two representative highly doped fibers (dashed curves). These simulated curves, which include the upconversion processes, fairly reproduce the experimental findings. Furthermore, the maximum relative amplitude and the corresponding intensity that gives that maximum value have been computed as a function of optical density for this value of κ . These simulated results are plotted in Figs. 2(b) and 2(c) (dashed curves), which clearly show the reduction of the grating efficiency obtained for the highly doped fibers showing good agreement with the experimental data.

4. CONCLUSIONS

We studied the efficiency of the dynamic population gratings recorded in highly doped erbium fibers via a transient TWM experiment. We analyzed the increase in the transmitted signals due to the self-diffraction of the recording signals in the grating. We find that grating efficiency increases with optical density, although fibers with large doping levels ($6.3 \times 10^{25} \text{ m}^{-3}$) exhibit lower efficiency than expected. Even so, the reflectivity reached in these highly doped fibers make possible the use of such fibers in many applications that require a minimization of fiber length without a reduction of the coupling efficiency. By measuring the backward fluorescence signal, we find an excitation quenching at these large doping levels. We also analyzed the behavior of the grating formation rate, which linearly increases with intensity. We obtain a slight increase of this slope for the highly doped fibers. We show that the reduction of the grating efficiency can be attributed to PIQ effects that appear at these high doping levels.

ACKNOWLEDGMENTS

We would like to thank fruitful discussions with S. Stepanov, M. Plata, M. Moreno and J. M. Ezquerro. This work has been

supported by projects FIS2007-65382 and FIS2010-22082 (Ministerio de Ciencia e Innovación) and GR58/08 910133-1030 (Santander Central Hispano-Universidad Complutense de Madrid) from Spain.

REFERENCES

1. S. Frisken, "Transient Bragg reflection gratings in erbium-doped fiber amplifiers," *Opt. Lett.* **17**, 1776–1778 (1992).
2. B. Fischer, J. L. Zyskind, J. W. Sulhoff, and D. J. DiGiovanni, "Nonlinear wave mixing and induced gratings in erbium-doped fiber amplifiers," *Opt. Lett.* **18**, 2108–2110 (1993).
3. M. Horowitz, R. Daisy, B. Fischer, and J. Zyskind, "Narrowlinewidth, single-mode erbium-doped fibre laser with intracavity wave mixing in saturable absorber," *Electron. Lett.* **30**, 648–649 (1994).
4. S. A. Havstad, B. Fischer, A. E. Willner, and M. G. Wickham, "Loop-mirror filters based on saturable-gain or -absorber gratings," *Opt. Lett.* **24**, 1466–1468 (1999).
5. S. Stepanov, E. Hernández, and M. Plata, "Two-wave mixing by means of dynamic Bragg gratings recorded by saturation of absorption in erbium-doped fibers," *Opt. Lett.* **29**, 1327–1329 (2004).
6. S. Stepanov, "Dynamic population gratings in rare-earth-doped optical fibres," *J. Phys. D* **41**, 224002 (2008).
7. S. Stepanov and E. Hernández, "Observation of spatial migration of excitation in Er-doped optical fibers by means of a population grating technique," *Opt. Lett.* **30**, 1926–1928 (2005).
8. S. Stepanov and E. Hernández, "Phase contribution to dynamic gratings recorded in Er-doped fiber with saturable absorption," *Opt. Commun.* **271**, 91–95 (2007).
9. S. Stepanov, E. Hernández, and M. Plata, "Two-wave mixing of orthogonally polarized waves via anisotropic population gratings in erbium-doped optical fiber," *J. Opt. Soc. Am. B* **22**, 1161–1166 (2005).
10. D. García Casillas and S. Stepanov, "Sub-milliwatt sub-millisecond recording of population gratings in ytterbium-doped optical fibers at 976 nm," *Opt. Commun.* **284**, 2202–2205 (2011).
11. S. Stepanov and M. Plata, "Slow and fast light via two-wave mixing in erbium-doped fibers with saturable absorption," *Phys. Rev. A* **80**, 053830 (2009).
12. L. F. Shampine, M. W. Reichelt, and J. Kierzenka, "Solving boundary value problems for ordinary differential equations in MATLAB with BVP4C," http://www.mathworks.com/bvp_tutorial.
13. F. Sanchez, P. L. Boudec, P.-L. Francois, and G. Stephan, "Effects of ion pairs on the dynamics of erbium-doped fiber lasers," *Phys. Rev. A* **48**, 2220–2229 (1993).
14. J. L. Wagener, P. F. Wysocki, M. J. F. Digonnet, H. J. Shaw, and D. J. DiGiovanni, "Effects of concentration and clusters in erbium-doped fiber lasers," *Opt. Lett.* **18**, 2014–2016 (1993).
15. P. F. Wysocki, J. L. Wagener, M. J. F. Digonnet, and H. J. Shaw, "Evidence and modelling of paired ions and other loss mechanisms in erbium-doped silica fibers," *Proc. SPIE* **1789**, 66–79 (1993).
16. J. Li, K. Duan, Y. Wang, W. Zhao, J. Zhu, Y. Guo, and X. Lin, "Modeling and effects of ion pairs in high-concentration erbium-doped fiber lasers," *J. Mod. Opt.* **55**, 447–458 (2008).
17. O. G. Calderón, S. Melle, F. Arrieta-Yáñez, M. A. Antón, and F. Carreño, "Effect of ion pairs in fast-light bandwidth in high concentration erbium-doped fibers," *J. Opt. Soc. Am. B* **25**, C55–C60 (2008).